Surface-Directed Spinodal Decomposition in Poly[3-hexylthiophene] and C_{61}-Butyric Acid Methyl Ester Blends

Yana Vaynzof,[†] Dinesh Kabra,[†] Lihong Zhao,[‡] Lay Lay Chua,[‡] Ullrich Steiner,[†] and Richard H. Friend[†,‡,*]

[†]Cavendish Laboratory, JJ Thomson Avenue, Cambridge-CB3 0HE, U.K. and [‡]Department of Physics, National University of Singapore, 117542 Singapore

ARTICLE

ABSTRACT Demixed blends of poly[3-hexylthiophene] (P3HT) and C61-butyric acid methyl ester (PCBM) are widely used in photovoltaic diodes (PV) and show excellent quantum efficiency and charge collection properties. We find the empirically optimized literature process conditions give rise to demixing during solvent (chlorobenzene) evaporation by spinodal decomposition. Ultraviolet photoemission spectroscopy (UPS) and X-ray photoemission spectroscopy (XPS) results are consistent with the formation of 1—2 nm thick surface layers on both interfaces, which trigger the formation of surface-directed waves emanating from both film surfaces. This observation is evidence that spinodal demixing (leading to a bicontinuous phase morphology) precedes the crystallization of the two components. We propose a model for the interplay of demixing and crystallization which explains the broadly similar PV performance for devices made with the bottom electrodes either as hole or electron collector. The process regime of temporal separation of demixing and crystallization is attractive because it provides a way to control the morphology and thereby the efficiency of PV devices.

KEYWORDS: bulk heterojunction photovoltaic cells · spinodal phase separation · photoemission spectroscopy · poly[3-hexylthiophene](P3HT) · C61-butyric acid methyl ester (PCBM)

Most polymer blend photovoltaic devices are made by spin-coating a two-component mixture from a common solvent. While the kinetics of binary polymer phase separation is reasonably well understood,[1] the prediction or analysis of the polymer phase morphologies in spin-cast films is complex because the rapid solvent evaporation typically leads to quenched blend morphologies which are far from equilibrium and which cannot be equilibrated on reasonable time scales.[2,3] In PV devices, the crystallization of one or both components further enhances the thermodynamic and morphological complexity of cast blends.[4] Despite a decade of intensive research a detailed understanding of the morphology-function relationship of organic electronic devices is still elusive.

In polymer film manufacture, the presence of the two film surfaces plays an important role during the phase separation process. In thermodynamic equilibrium, surface wetting layers reflect surface tension differences between the binary components. These surface tension differences drive surface-directed composition waves when the blend film is quenched from a mixed state in the melt.[5,6] While these thermodynamic mechanisms are reasonably well understood, they are not necessarily applicable to blends containing conjugated polymers and nonpolymeric compounds. When cast from a solution, phase morphologies often evolve from an initially stratified bilayer,[7] which was recently demonstrated for generic polymer blend[8] and photoactive mixtures.[9] Furthermore, the interplay of demixing and polymer crystallization is expected to have a significant impact on nano- and micrometer scale blend morphologies in PV devices.

Gaining control over bulk and surface morphologies in PV blend is expected to have a profound effect on their performance. Ideally, such a blend should form a bicontinuous (possibly crystalline) morphology in the bulk with a characteristic domain size that is comparable to the exciton diffusion length (~10 nm). Near the electrodes, the enrichment of the electronically favorable component can be of advantage, while such an enrichment of the unfavorable component is likely to adversely affect PV performance. Any additional layering parallel to the electrodes within the device is also unfavorable. Despite the large number of publications on the preparation of photoactive polymer blends, the full complexity of these binary systems is not understood.

In terms of film surface layers in PV-devices, the role of a partially stratified phase morphology should affect the

*Address correspondence to rhf10@cam.ac.uk.

Received for review October 26, 2010 and accepted December 15, 2010.

Published online December 28, 2010. 10.1021/nn102899g

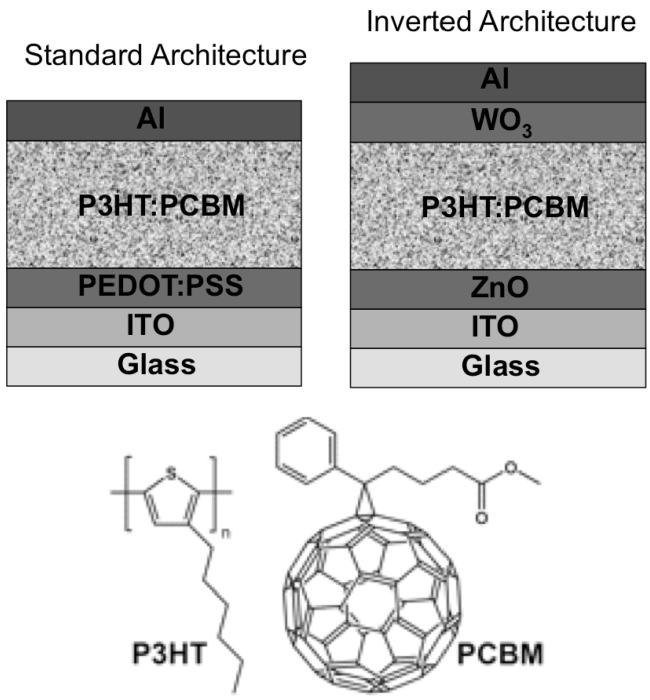

Figure 1. A schematic drawing showing the structure of a typical standard architecture device and the structure of the inverted photovoltaic device studied in this work. Below are the chemical structure of the P3HT polymer and PCBM molecule.

performance of the "standard architecture" device, in which the substrate provides the bottom contact serving as an anode and the top contact as a cathode, compared to the "inverted architecture" (Figure 1). The benefit of either architecture remains an open question. Both architectures have been investigated by numerous research groups, employing a range of model active systems. Though the inverted structure undoubtedly offers increased stability and does not require the use of the highly acidic poly(3,4-ethylenedioxythiophene) poly(styrenesulfonate) PEDOT:PSS,[10,11] it remains unclear which architecture is favorable in terms of device performance. Despite the recent reports that vertical phase separation of P3HT and PCBM is advantageous for inverted architecture devices, similar efficiencies have been reported for the two architectures.[12,13]

Very recently studies have emerged, linking aspects of blend morphologies in thin films to PV device performance. Using dynamic secondary ion mass spectrometry, Moons and co-workers have detected the presence of a surface directed spinodal wave in spin-cast polyfluorene:C61-butyric acid methyl ester blends.[14] Despite the formation of electronically unfavorable layer sequence, surface-directed demixing led to an improved PV-device performance.

In the case of one of the most successful PV blends of poly[3-hexylthiophene] (P3HT) and C61-butyric acid methyl ester (PCBM), the role of demixing in thin films is less clear. Several studies have established the enrichment of P3HT at the free surface and PCBM adjacent to various transparent conducting substrate materials, but none of these studies provides insight into the formation of these layers. Ellipsometry measurements by Campoy-Quiles *et al.*[15] suggest the formation of laterally and vertically phase separated P3HT:PCBM morphology that is driven by P3HT crystallization and subsequent PCBM diffusion. They postulate the formation of linear composition gradients across the film, aiding the PV-performance. Similar composition gradients are also found by Loos and co-workers using electron tomography, albeit with an inverted direction (*i.e.*, with P3HT enrichment at the substrate interface). P3HT:PCBM surface composition has also been studied by electron tomography[16] and dynamic SIMS.[17] Recent neutron reflectivity studies by Mackay *et al.* and Jones *et al.* confirm P3HT and PCBM surface enrichment but these authors do not explain how these structures are formed.[8,18]

This study contributes toward a better understanding of structure formation in P3HT/PCBM films and examines its consequences on regular and inverted device geometries.

We first examined thin films of P3HT, PCBM, and P3HT:PCBM spin-cast from chlorobenzene onto ZnO by means of UPS revealing the formation of thin pure layers of P3HT and PCBM at the air and substrate surfaces of the blend film, respectively.

To probe the bulk composition, P3HT:PCBM blend films of various thicknesses were imaged by XPS depth profiling. This technique combines XPS, which probes the chemical composition of the surface with an Ar ion gun sputtering away material to achieve vertical resolution, thereby allowing direct measurement of the film composition depth profile. This technique was previously used to reveal the composition profiles of conducting polymer blends such as PEDOT:PSS[19] and polyaniline:poly (2-acrylamido-2-methyl-1-propanesulfonic acid) (PANI: PAAMPSA).[20]

Finally, we fabricated inverted architecture photovoltaic devices of similar thicknesses to the ones studies by XPS depth profiling and characterized their performance.

RESULTS AND DISCUSSION

Vertical Phase Separation Studies—Top and Bottom Film Surfaces. We examine the vertical phase separation in blend films, first by means of ultraviolet photoemission spectroscopy (UPS) for thin ~10 nm thick films. The UPS measurements allow us to examine the energy level alignment between the organic layers and the ZnO substrate. The work function (WF) of the bare ZnO substrate is 3.6 eV, indicating that the ZnO Fermi (E_F) level lies within the conduction band.[21] UPS spectra were collected from P3HT/ZnO and PCBM/ZnO samples. As can be seen in Figure 2, the secondary photoemission onset measured on the P3HT matches, within the experimental resolution, the onset measured on the underlying substrate (Figure 2a). This cor-

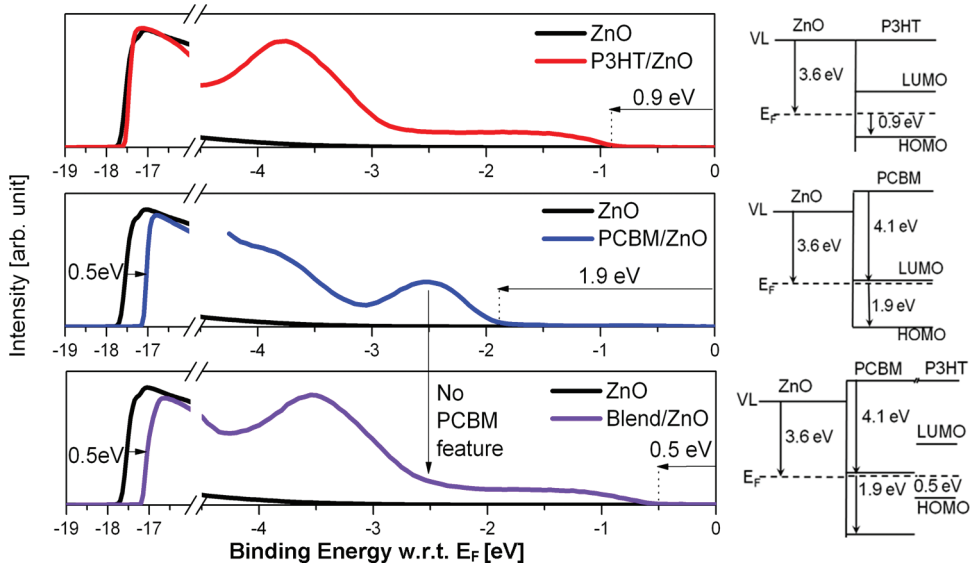

Figure 2. (a) UPS spectra of ZnO (black) and P3HT/ZnO (red), (b) UPS spectra of ZnO (black) and PCBM/ZnO (blue), (c) UPS spectra of ZnO (black) and P3HT:PCBM/ZnO (purple) with corresponding energy level diagrams.

responds to vacuum level alignment between the P3HT polymer and substrate. In the case of PCBM/ZnO, the WF is increased by 0.5 eV to a value of 4.1 eV (Figure 2b). We interpret this increase in WF as an interfacial dipole pointing away from the ZnO substrate, corresponding to a ground state electron charge transfer from the ZnO to the PCBM. The low binding energy edge of the polymer valence band corresponds to the position of the highest occupied molecular orbital (HOMO).[22] We measure the positions of the P3HT and the PCBM HOMOs to be 0.9 and 1.9 eV below the Fermi level, respectively. Energy level diagrams are summarized in Figure 2. In the case of a P3HT:PCBM/ZnO sample, we measure a WF of 4.1 eV, the same as for PCBM/ZnO (Figure 2c). We consider this to result from PCBM accumulation near the ZnO substrate, as has been previously observed for Cs_2CO_3/ITO substrates.[23] The HOMO edge measured on the blend/ZnO sample is found to be 0.5 eV below the Fermi level. The valence band spectra for the blend/ZnO show no PCBM features, indicating that pure P3HT is formed on the surface of the blend film. This agrees with previous reports of P3HT accumulation at the top surface due to its lower surface energy.[24] We assign the blend HOMO to be the P3HT HOMO. This is corroborated by the ionization potential (IP) calculated from the blend/ZnO UPS spectrum, which we find to be 4.6 eV, in agreement with previously measured values for pure P3HT.[25] UPS measurements therefore show that for thin films there is accumulation of PCBM at the ZnO surface and of P3HT at the top surface.

Vertical Phase Separation Studies—Bulk Depth Profiling. We use an XPS depth profiling technique to probe the composition variation in thicker films, probing chemical surface composition with XPS and using ion gun sputtering of the film to achieve depth resolution. We note that that the technique does not provide lateral resolution, as the XPS signal is collected from the entire sample area. In the case of the P3HT:PCBM blend, the P3HT to PCBM weight ratio can be calculated from the S/C atomic ratios, but S/O atomic ratios prove to be unreliable due to oxygen contamination in the sample. To calibrate the sputtering rate and to estimate the damage in the sample upon sputtering, a 50 nm thick P3HT film on Au was sputtered and the S/C ratio was calculated at 14 stages of sputtering throughout the sample thickness. The S/C ratio was found to be 0.118 ± 0.008, in agreement with Ponjee *et al.*[26] When using a gentle sputtering rate (0.3 nm/min), the consistency in the P3HT stoichiometry throughout the sputtering process indicates that the damaged material is sputtered away so that only the very top surface is perturbed. The XPS signal comes from a depth of 4−5 nm, which remains unaffected by the sputtering process, so that the XPS

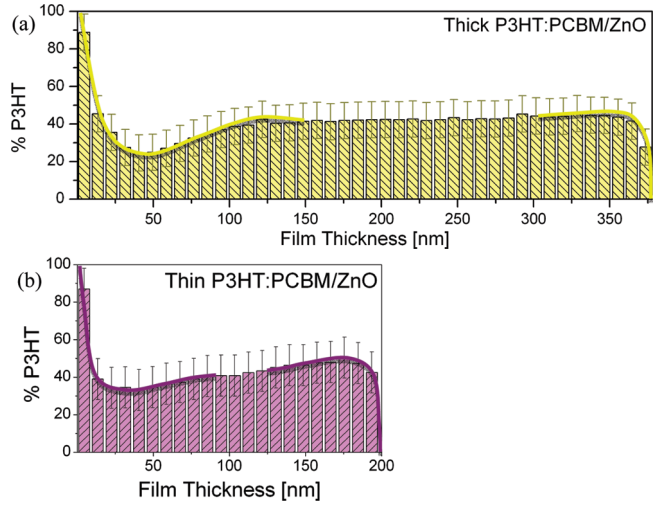

Figure 3. (a) XPS depth profile obtained on ~370 nm thick P3HT:PCBMfilm on ZnO, (b) XPS depth profile obtained on ~200 nm thick P3HT:PCBM film on ZnO. Solid lines are guidelines for spinodal waves originating from the bottom and top surfaces.

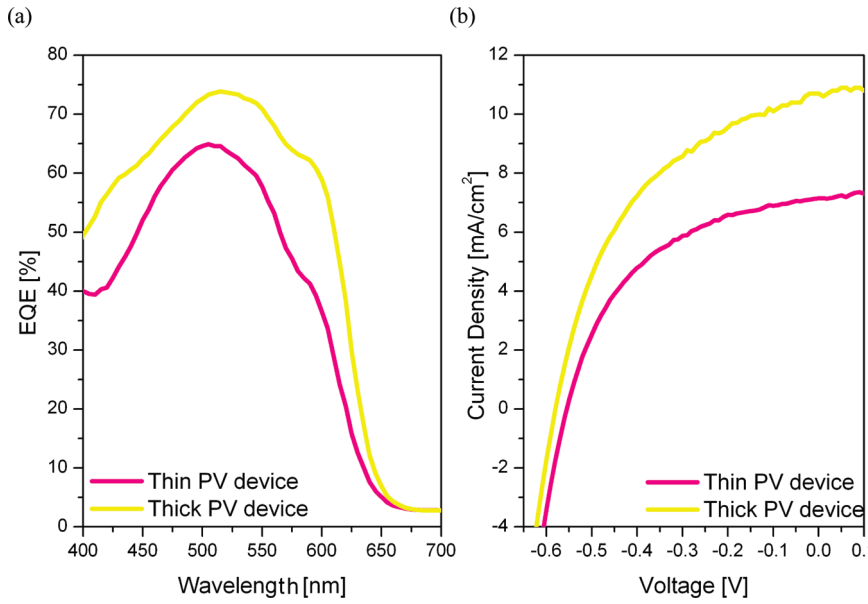

Figure 4. (a) EQE of 200 and 370 nm thick inverted architecture PV devices with P3HT:PCBM active layers. (b) *I*−*V* curves measured under a solar simulator.

data provides a reliable measurement of the sample composition as a function of probing depth. When sputtering a P3HT:PCBM blend film, we believe that the sputtering rate for P3HT and PCBM to be sufficiently similar as both materials are fairly similar in composition.

The vertical composition profile of a ~370 nm thick sample is shown in Figure 3a. As expected from the UPS results, the top surface of the blend film (depth 0) is P3HT rich. XPS measurements taken on very thin UPS samples also show a thin P3HT top surface layer. The P3HT surface layer is followed by P3HT depletion, reaching a minimum at a depth of ~40 nm below the surface. The concentration reaches a constant value at ~120 nm, which remains constant until the substrate interface where it falls off, in agreement with the PCBM accumulation at the bottom surface observed with UPS. The results for the thinner ~200 nm sample are presented in Figure 3b. As in the previous case, the top surface is P3HT rich, followed by P3HT depletion, with a minimum at ~40 nm. The P3HT concentration increases as we probe closer to the ZnO interface. Our results indicate that the XPS depth profiling method can provide us with accurate vertical phase composition profiles with a depth resolution of 10−20 nm near the substrate that is set by the increasing roughness of the sputtered surface as it is progressively removed by the sputtering.

Inverted Photovoltaic Device Performance. We examined the performance of photovoltaic (PV) devices with similar thicknesses fabricated in an inverted architecture on ZnO/ITO substrates. The external quantum efficiency (EQE) curves of devices with thickness of ~200 and ~370 nm are shown in Figure 4a. The maximum EQE is observed at a wavelength of 510 nm and is 76% for the thicker device, and 65% for the thinner device. We note that 76% EQE corresponds to ~100% internal quantum efficiency (IQE), showing that all the photogenerated charge carriers were successfully collected. The current−voltage characteristics show that the short circuit current (J_{sc}) of the thin device is ~30% smaller than that of the thicker device (Figure 4b). We note that this is in contrast to "standard" devices, in which increasing the active layer thickness lowers the device performance.[27] The overall device performance parameters are summarized in Table 1.

DISCUSSION

The combined UPS and XPS results are consistent with a very thin P3HT surface layer, which is nearly P3HT-pure directly at the surface. As UPS is far more surface sensitive than XPS (resolution 1−2 nm), it allows us to estimate the thickness of the top P3HT layer to be 1−2 nm, in agreement to findings by Xu *et al.*[11] This surface layer is followed by an ~80 nm wide P3HT depletion zone. While the XPS resolution at the substrate is lower, UPS reveals a similarly thin PCBM layer at the ZnO substrate followed by a wider PCMB depletion zone (Figure 3b). A comparison to ref 27 reveals a striking similarity to surface-spinodal waves emanating from the two surfaces. Such surface spinodal waves typically

TABLE 1. V_{oc}, J_{sc}, FF, and Power Conversion Efficiency η of 200 and 370 nm Thick Inverted Architecture PV Devices with P3HT:PCBM Active Layers under AM1.5 Solar Simulator Conditions (100 mW/cm²)

	J_{sc}(mA/cm²)	V_{oc}(V)	FF (%)	η (%)
thin PV device	7.15	0.56	47.9	1.91
thick PV device	10.7	0.59	45.9	2.9

consist of a very thin, often continuous, enrichment layer in direct contact with the surface, followed by a longer-wavelength wave, which mirrors the characteristic spinodal wavelength in the bulk.

We therefore interpret our results in the framework of "surface-directed spinodal decomposition" in polymer blends. The preferential attraction of one of the blend components at the surface causes the formation of a thin adsorption layer which triggers spinodal decomposition waves with a preferred wave vector orientation normal to the surface, breaking the spatial isotropy of composition fluctuations in the bulk. In the case of P3HT:PCBM blends, P3HT tends to accumulate at the free surface, lowering the surface energy of the blend, while PCBM accumulates near the polar ZnO surface. This results in two spinodal waves propagating from the top and bottom surfaces into the film bulk. The results for the thinner P3HT:PCBM sample demonstrate this phenomenon particularly clearly. While the spinodal P3HT wave at the top surface is evident, the P3HT enhancement seen near the substrate is indicative of PCMB adsorption at the substrate, triggering a PCBM spinodal wave. The 370 nm thick sample, also shows a P3HT spinodal wave originating from the top surface, but the PCBM wave is probably obscured by the lowered depth resolution for the thicker film.

The surface spinodal wave is expected to match the characteristic spinodal length scale that develops in the bulk of the sample upon quenching. While the surface spinodal mode is affected by surface energy differences of the blend components and its stratified topology, experiments[28] and model calculations[29] show that the wavelength of surface spinodal mode, while somewhat smaller, closely approximates the bulk spinodal mode. The wavelength of the surface spinodal wave of $\lambda \approx 80$ nm corresponds to a wavenumber $q_m = 2\pi/\lambda \approx 8 \times 10^{-3}$ Å^{-1} for both film thicknesses. This is in good agreement with the value of $\sim 6 \times 10^{-3}$ Å^{-1}, measured by grazing-incidence small-angle X-ray scattering (GISAXS) by Chiu *et al.*[30]

The observation of surface-directed spinodal decomposition is interesting because it allows us to draw a number of conclusions concerning the evolution of P3HT:PCBM phase morphology and crystallization. The existence of a spinodal pattern suggests that structure formation in the P3HT:PCBM blend is initiated by a binary demixing process. In particular, the existence of a 80 nm surface-oriented wave rules out a phase separation process that is driven by P3HT crystallization, which would lead to much smaller structures.

Binary demixing will, however, only lead to the good electronic properties of the P3HT:PCBM blend that we see if the resulting blend morphology is bicontinuous. For solution mixtures of symmetric P3HT:PCBM composition, a bicontinuous morphology upon demixing necessitates a comparable solubility of the two components. The importance of a symmetric solubility for P3HT:PCBM device manufacture was recently reported by Troshin and co-workers.[31] Our observation of P3HT:PCBM demixing explains this requirement.

In addition to a bicontinuous phase morphology, good photovoltaic performance requires P3HT crystallization and the formation of PCMB aggregates or crystals. This raises the question of the interplay of demixing and phase separation. Following arguments by Hu and Frenkel[32] and recent experimental work on polyolefins by Han,[33] several simple statements can be made. While crystallization is a nucleated process with an associated energy barrier, spinodal demixing is spontaneous and not subject to an energetic barrier. If the critical point for demixing is higher or comparable to the melting point, quenching a blend from a homogeneous melt or solution therefore initially results in the spinodal demixing into two coexisting phases. The onset of crystallization is a secondary process that sets in once the coexisting phase morphology has formed. Han has reported two interesting observations for a binary polefin blend with one crystallizable component: (1) Compared to a crystallizing one-component system, crystal nucleation is greatly accelerated by the demixing of the same crystallizing component in a binary blend. (2) Crystals are nucleated at the phase boundaries driven both by kinetic[32] and energetic effects.[34]

Crystallization of P3HT and PCBM within the phase-separated structure must lead to a secondary demixing process on a much smaller (~10 nm) length scale. This is the necessary consequence of the fact that the coexisting phases are pure only in the zero-temperature limit, while the crystals are phase-pure. This interplay of well-defined demixing and crystallization is supported by the work of researchers[35] who have reported an eutectic behavior of the P3HT:PCBM blend, which requires the well controlled fractional mixing of the two components.

While the XPS measurements provide no information about the bulk morphology in the interior part of the film, our conclusions concerning bicontinuous spinodal followed by secondary P3HT crystallization are a combination of the observations of Figure 3 with the structural prerequisites for a good photovoltaic performance. A combination of our results with earlier published work allows the reconstruction of the detailed morphology within the P3HT:PCBM active layer. The effect of morphology on photovoltaic performance is an important issue and has been subject to numerous studies.[36,37] Our proposed model is summarized in Figure 5: (1) During film formation thin PCBM and P3HT surface layers form at the substrate and free surfaces, respectively. (2) These surface layers trigger a surface spinodal wave, which connects to (3) a cocontinuous binary morphology within the film. P3HT/PCBM phase separation triggers (4) interfacial crystallization, thereby creating a secondary, smaller phase morphology. Although we do not offer direct evidence of interfacial

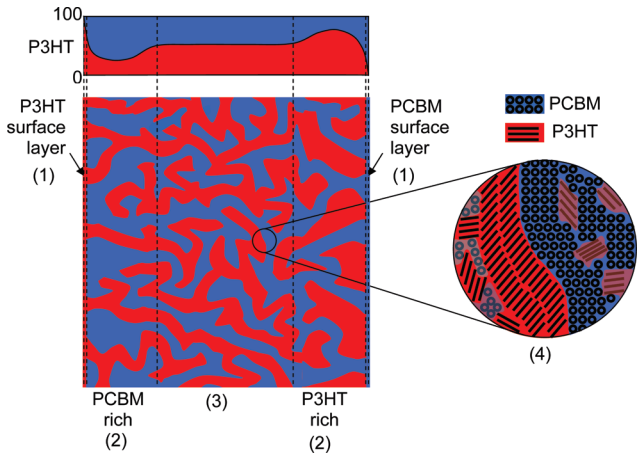

Figure 5. Schematic diagram of the detailed morphology within the P3HT:PCBM active layer: (1) During film formation thin PCBM and P3HT surface layers form at the substrate and free surfaces, respectively. (2) These surface layers trigger a surface spinodal wave, which connects to (3) a cocontinuous binary morphology within the film. P3HT/PCBM phase separation triggers (4) interfacial crystallization, thereby creating a secondary, smaller phase morphology.

crystallization occurring in the P3HT:PCBM system, this is supported by observation of Han *et al.* as discussed above.[33]

The photovoltaic consequences of this self-organized structure are intriguing. Devices with similar power conversion efficiencies have been reported both for the standard and inverted architecture. This is surprising in the context of the surface layering reported here. The build-up of standard devices benefit from P3HT enrichment at the (PEDOT:PSS) substrate surface and PCBM enrichment at the free surface (*i.e.*, the Al electrode). The inverted device on the other hand benefits from PCBM/P3HT layering on the substrate (ZnO)/free (WO_3) surface, respectively.

This suggests that details of the device manufacture and architecture might be important. In particular, assuming that the subsurface (80 nm) waves are not laterally continuous, the existence of the thin (1−2 nm) surface layers is disadvantageous for the standard device. However, both thin layers are easily destabilized by further device processing. The top P3HT layer, for example, may be perturbed during electrode evaporation[38] and postannealing processes.[39] The bottom 1 nm thick PCBM layer can similarly be perturbed by further annealing steps. Alternatively, the formation of substrate layer can be controlled by varying the surface chemistry to correctly contact the bottom electrode of either architecture device.[40,41] The break-up of these extremely thin layers leaves only small amounts of the antagonistic material at the two electrodes, exposing them to subsurface waves resulting in an equally favorable composition for both device architectures.

In the bulk, the bicontinuous demixing morphology enables efficient charge transport to electrodes. Within the domains, interface-driven crystallization is favorable because it aligns the crystal morphologies with respect to the binary interfaces thereby enabling exciton migration to the interface followed by effective charge separation.

CONCLUSIONS

The experimental results presented here are clear evidence that the casting of a symmetrical P3HT:PCBM film from chlorobenzene results in the phase separation of the two components with a relatively large domain size. Combining our experimental results with earlier published work, we present a model for structure formation in this photovoltaic mixture, summarized in Figure 5. Film-casting of the mixture from chlorobenzene gives rise to surface-directed spinodal decomposition, with the formation of 1−2 nm thick pure P3HT and PCBM layers at the air and ZnO surfaces, respectively. The observation of an ~80 nm wide composition wave adjacent to these surface layers in combination with the good photovoltaic performance of the device leads us to the conclusion of a bicontinuous P3HT:PCBM morphology within the film as a result of spinodal decomposition. Comparison to the interplay of phase separation and crystallization in polyolefin systems suggests the formation of interface-directed crystallization (or aggregate formation) of the two components.

The resulting hierarchical morphology is conceptually highly beneficial for the photovoltaic performance of the blend: interfacial crystal alignment should facilitate exciton dissociation, while a bicontinuous mesomorphology enables efficient charge extraction.

The kinetic structure formation pathway provides the opportunity for the tuning of the P3HT:PCBM photovoltaic blends based on principles that are well established in polymer science: (1) the formation of surface-enriched layers can be controlled by surface modification and the use of surface-anchors; (2) the bicontinuous domains size can be adjusted by a variation of the film-formation kinetic or the use of surfactants,[42] and (3) the P3HT (and possibly PCBM) crystallization kinetics and morphology can be tuned by a postcasting solvent-vapor annealing step. The simultaneous control of these parameters is a challenging but viable route toward the further improvement of P3HT:PCBM device performance.

EXPERIMENTAL METHODS

Patterned ITO substrates were sonicated in acetone (15 min) and IPA (15 min) consecutively. Thin films of ZnO were deposited by means of spray pyrolysis deposition (SPD) from an 80 g/L zinc acetate dihydrate (Fluka) in methanol solution.[43] The samples were annealed at 350 °C in air for 15 min. For the ultraviolet photoemission spectroscopy (UPS) studies, the P3HT (Rieke Metals, M_w = 50000−60000 g/mol, RR = 92−93%) and PCBM (Solenne) were weighed in air and dissolved in anhydrous chlorobenzene (CB) at 70 °C overnight to spin-coat thin films

(~10 nm) of P3HT, PCBM, and P3HT:PCBM 1:1 weight-ratio blends. For X-ray photoemission spectroscopy (XPS) depth profiling studies as well as for photovoltaic devices (PVs) concentrations of 35 and 48 mg/mL were used either to spin coat thin films (~200 nm) or thick films (~370 nm). The film thicknesses were determined using a Dektak profilometer. The organic layers were spin coated from a hot solution using a two-step spinning process: first, at a speed of 600 rpm for 300 s and then immediately at 3000 rpm for an additional 60 s.

The PES samples were annealed at 130 °C for 15 min in order to remove residual solvent and transferred to the ultrahigh vacuum (UHV) chamber (VG ESCALAB MK-II) for UPS/XPS measurements. The PV samples were transferred to a thermal evaporation chamber for WO_3 (10 nm), Ag (30 nm), and Al (60 nm) deposition under high vacuum (1×10^{-6} mbar). Finally, the samples were post annealed at 130 °C for 15 min.

UPS measurements were performed using the He I photon line ($h\nu = 21.22$ eV) of a He discharge lamp under UHV conditions (4×10^{-10} mbar). Emitted photoelectrons were collected using a semispherical channeltron with analyzer pass energy set to 5 eV. During data collection the samples were biased at −10 V in order to measure the onset of the photoemission spectra, which is used to determine the position of the vacuum level. The analyzer resolution was confirmed by Fermi-step of atomically cleaned gold-foil to be 0.15 eV. An Ar+ ion gun was used for sputtering experiments at an ionization energy of 2 kV. The beam was defocused to cover the entire sample area. The sputtering rate was estimated to be approximately 0.3 nm/min. XPS was carried out with the Mg Kα line ($h\nu = 1253.6$ eV) with analyzer pass energy of 10 eV.

For external quantum efficiency (EQE) measurements (in air) a 100 W halogen lamp and a Bentham monochromator were used. The measurements were performed as a function of wavelength at intensities of ~1mW/cm^2. To measure the $I-V$ curve of the device under AM1.5 conditions, an Oriel 81160−1000 solar cell simulator was used. To obtain reliable data, a spectral mismatch correction is carried out using a calibrated and certified inorganic solar cell.

Acknowledgment. We thank the UK Engineering and Physical Sciences Research Council for support. We would like to thank H. K. Wong for technical help during the photoemission measurements.

REFERENCES AND NOTES

1. Strobl, G. R. *The Physics of Polymers: Concepts for Understanding Their Structures and Behavior*, 3rd ed.; Springer: New York, 1997.
2. Barbero, D. R.; Steiner, U. Nonequilibrium Polymer Rheology in Spin-Cast Films. *Phys. Rev. Lett.* **2009**, *102*, 248303.
3. Raegen, A.; Chowdhury, M.; Calers, C.; Schmatulla, A.; Steiner, U.; Reiter, G. Aging of Thin Polymer Films Cast from a Near-Theta Solvent. *Phys. Rev. Lett.* **2010**, *105*, 227801.
4. Bjorstrom Svanstrom, C. M.; Rysz, J.; Bernasik, A.; Budkowski, A.; Zhang, F.; Inganas, O.; Andersson, M. R.; Magnusson, K. O.; Benson-Smith, J. J.; Nelson, J.; *et al.* Device Performance of APFO-3/PCBM Solar Cells with Controlled Morphology. *Adv. Mater.* **2009**, *21*, 4398–4403.
5. Kim, E.; Krausch, G.; Kramer, E.; Osby, J. O. Surface-Directed Spinodal Decomposition in the Blend of Polystyrene and Tetramethyl-Bisphenol-A Polycarbonate. *Macromolecules* **1994**, *27*, 5927–5929.
6. Geoghegan, M.; Jones, R. A. L.; Clough, A. S. Surface Directed Spinodal Decomposition in a Partially Miscible Polymer Blend. *J. Chem. Phys.* **1995**, *103*, 2719.
7. Walheim, S.; Böltau, M.; Mlynek, J.; Krausch, G.; Steiner, U. Structure Formation *via* Polymer Demixing in Spin-Cast Films. *Macromolecules* **1997**, *30*, 4995–5003.
8. Heriot, S. Y.; Jones, R. A. L. An Interfacial Instability in a Transient Wetting Layer Leads to Lateral Phase Separation in Thin Spin-Cast Polymer-Blend Films. *Nat. Mater.* **2005**, *4*, 782–786.
9. Jukes, P. C.; Heriot, S. Y.; Sharp, J. S.; Jones, R. A. L. Time-Resolved Light Scattering Studies of Phase Separation in Thin Film Semiconducting Polymer Blends during Spin-Coating. *Macromolecules* **2005**, *38*, 2030–2032.
10. Kawano, K.; Pacios, R.; Poplavskyy, D.; Nelson, J.; Bradley, D. D. C.; Durrant, J. R. Degradation of Organic Solar Cells Due to Air Exposure. *Sol. Energy Mater. Sol. Cells* **2006**, *90*, 3520.
11. Liao, H. -H; Chen, L. -M; Xu, Z.; Li, G.; Yang, Y. Highly Efficient Inverted Polymer Solar Cell by Low Temperature Annealing of Cs_2CO_3 Interlayer. *Appl. Phys. Lett.* **2008**, *92*, 173303.
12. Xu, Z.; Chen, L. -M; Yang, G.; Huang, C. -H; Hou, J.; Wu, Y.; Li, G.; Hsu, C. -S; Yang, Y. Vertical Phase Separation in Poly(3-hexylthiophene):Fullerene Derivative Blends and Its Advantage for Inverted Structure Solar Cells. *Adv. Funct. Mater.* **2009**, *19*, 1227–1234.
13. Li, G.; Shrotriya, V.; Huang, J.; Yao, Y.; Moriarty, T.; Emery, K.; Yang, Y. High-Efficiency Solution Processable Polymer Photovoltaic Cells by Self-Organization of Polymer Blends. *Nat. Mater.* **2005**, *4*, 864–868.
14. Nilsson, S.; Bernasik, A.; Budkowski, A.; Moons, E. Morphology and Phase Segregation of Spin-Casted Films of Polyfluorene/PCBM Blends. *Macromolecules* **2007**, *40*, 8291–8301.
15. Campoy-Quiles, M.; Ferenczi, T.; Agostinelli, T.; Etchegoin, P. G.; Kim, Y.; Anthopoulos, T. D.; Stavrinou, P. N.; Bradley, D. D. C.; Nelson, J. Morphology Evolution *via* Self-Organization and Lateral and Vertical Diffusion in Polymer: Fullerene Solar Cell Blends. *Nat. Mater.* **2008**, *7*, 158–164.
16. Bavel, S. S. V.; Sourty, E.; With, G. D; Loos, J. Three-Dimensional Nanoscale Organization of Bulk Heterojunction Polymer Solar Cells. *Nano Lett.* **2009**, *9*, 507–513.
17. Yu, B. -Y; Lin, W. -C; Wang, W. -B; Iida, S. -I; Chen, S. -Z; Liu, C. -Y; Kuo, C. -H; Lee, S. -H; Kao, W. -L; Yen, G. -J; *et al.* Effect of Fabrication Parameters on Three-Dimensional Nanostructures of Bulk Heterojunctions Imaged by High-Resolution Scanning ToF-SIMS. *ACS Nano* **2010**, *4*, 833–840.
18. Kiel, J. W.; Kirby, B. J.; Majkrzak, C. F.; Maranvillec, B. B.; Mackay, M. E. Nanoparticle Concentration Profile in Polymer-Based Solar Cells. *Soft Matter* **2010**, *6*, 641–646.
19. Hwang, J.; Ami, F.; Kahn, A. Spectroscopic Study on Sputtered PEDOT:PSS: Role of Surface PSS Layer. *Org. Electron.* **2006**, *7*, 387–396.
20. Yoo, J. E.; Krekelberg, W. P.; Sun, Y.; Tarver, J. D.; Truskett, T. M.; Loo, Y.-L. Polymer Conductivity through Particle Connectivity. *Chem. Mater.* **2009**, *21*, 1948–1954.
21. Allen, M. W.; Swartz, C. H.; Myers, T. H.; Veal, T. D.; McConville, C. F.; Durbin, S. M. Bulk Transport Measurements in ZnO: The Effect of Surface Electron Layers. *Phys. Rev. B* **2010**, *81*, 075211.
22. Kahn, A.; Koch, N.; Gao, W. Electronic Structure and Electrical Properties of Interfaces between Metals and π-Conjugated Molecular Films. *J. Polym. Sci., Part B* **2003**, *41*, 2529.
23. Xu, Z.; Chen, L.-M.; Chen, M.-H.; Li, G.; Yang, Y. Energy Level Alignment of Poly(3-hexylthiophene): [6,6]-Phenyl C_{61} Butyric Acid Methyl Ester Bulk Heterojunction. *Appl. Phys. Lett.* **2009**, *95*, 013301.
24. Guan, Z.-L; Kim, J. B.; Wang, H.; Jaye, C.; Fischer, D. A.; Loo, Y. -L; Kahn, A. Direct Determination of the Electronic Structureof the Poly(3-hexylthiophene):Phenyl-[6,6]-C_{61} Butyric Acid Methyl Ester Blend. *Org. Electron.* **2010**, *11*, 1779–1785.
25. Osikowicz, W.; de Jong, M. R.; Salaneck, W. R. Formation of the Interfacial Dipole at Organic−Organic Interfaces: C_{60}/Polymer Interfaces. *Adv. Mater.* **2007**, *19*, 4213.
26. Ponjee, M. W. G.; Reijme, M. A.; Langeveld-Voss, B. M. W.; Danier van der Gon, A. W.; Brongersma, H. H. Molecular Surface Structure of Poly(3-hexylthiophene) Studied by Low Energy Ion Scattering. *Surf. Sci.* **2002**, *512*, 194–200.

27. Kim, M.-S.; Kim, B.-G.; Kim, J. Effective Variables To Control the Fill Factor of Organic Photovoltaic Cells. *ACS Appl. Mater. Interfaces* **2009**, *1* (6), 1264–1269.
28. Jones, R. A. L.; Norton, L. J.; Kramer, E. J.; Bates, F. S.; Wiltzius, P. Surface-Directed Spinodal Decomposition. *Phys. Rev. Lett.* **1991**, *66*, 1326–1329.
29. Puri, S.; Binder, K. Surface Effects on Spinodal Decomposition in Binary Mixtures and the Interplay with Wetting Phenomena. *Phys. Rev. E* **1994**, *49*, 5359–5377.
30. Chiu, M.-Y; Jeng, U.-S.; Su, C.-H.; Liang, K. S.; Wei, K.-H. Simultaneous Use of Small- and Wide-Angle X-ray Techniques to Analyze Nanometerscale Phase Separation in Polymer Heterojunction Solar Cells. *Adv. Mater.* **2008**, *20*, 2573–2578.
31. Troshin, P. A.; Hoppe, H.; Renz, J.; Egginger, M.; Moyarove, J. Y.; Goryachev, A. E.; Peregudov, A. S.; Lyubovskaya, R. N.; Gobsch, G.; Sariciftci, N. S.; *et al*. Material Solubility-Photovoltaic Performance Relationship in the Design of Novel Fullerene Derivatives for Bulk Heterojunction Solar Cells. *Adv. Funct. Mater.* **2009**, *19*, 779–788.
32. Hu, W.; Frenkel, D. Polymer Crystallization Driven by Anisotropic Interactions. *Adv. Polym. Sci.* **2005**, *191*, 1–35.
33. Zhang, X.-H.; Wang, Z.-G.; Dong, X.; Wang, D.-J.; Han, C. C. Interplay between Two Phase Transitions: Crystallization and Liquid−Liquid Phase Separation in a Polyolefin Blend. *J. Chem. Phys.* **2006**, *125*, 024907.
34. Ma, Y.; Zha, L.; Hu, W.; Reiter, G.; Han, C. C. Crystal Nucleation Enhanced at the Diffuse Interface of Immiscible Polymer Blends. *Phys. Rev. E* **2008**, *77*, 061801.
35. Muller, C.; Ferenczi, T. A. M.; Campoy-Quiles, M.; Frost, J. M.; Bradley, D. D. C.; Smith, P.; Stingelin-Stutzmann, N.; Nelson, J. Binary Organic Photovoltaic Blends: A Simple Rationale for Optimum Compositions. *Adv. Mater.* **2008**, *20*, 3510–3515.
36. Hoppe, H.; Sariciftci, N. S. Morphology of Polymer/Fullerene Bulk Heterojunction Solar Cells. *J. Mater. Chem.* **2006**, *16*, 45–61.
37. Ballantyne, A. M.; Ferenczi, T. A.; Campoy-Quiles, M.; Clarke, T. M.; Maurano, A.; Wong, K. H.; Zhang, W.; Stingelin Stutzmann, N.; Kim, J.-S.; Bradley, D. D. C.; *et al.* Understanding the Influence of Morphology on Poly(3-hexylselenothiophene):PCBM Solar Cells. *Macromolecules* **2010**, *43*, 1169–1174.
38. Wang, M.; Tang, Q.; An, J.; Xie, F.; Chen, J.; Zheng, S.; Wong, K. Y.; Miao, Q.; Xu, J. Performance and Stability Improvement of P3HT:PCBM-Based Solar Cells by Thermally Evaporated Chromium Oxide (CrOx) Interfacial Layer. *ACS Appl. Mater. Interfaces* **2010**, *2*, 2699–2702.
39. Ma, W.; Yang, C.; Gong, X.; Lee, K.; Heeger, A. J. Thermally Stable, Efficient Polymer Solar Cells with Nanoscale Control of the Interpenetrating Network Morphology. *Adv. Funct. Mater.* **2005**, *15*, 1617–1622.
40. Germack, D. S.; Chan, C. K.; Hamadani, B. H.; Richter, L. J.; Fischer, D. A.; Gundlach, D. J.; DeLongchamp, D. M. Substrate-Dependent Interface Composition and Charge Transport in Films for Organic Photovoltaics. *Appl. Phys. Lett.* **2009**, *94*, 233303.
41. Wang, H.; Gomez, E.; Guan, Z.; Kahn, A.; Jaye, C.; Fischer, D.; Schwartz, J.; Loo, Y.-L. Elucidating Vertical Phase Separation of Active Layers in Polymer Solar Cells *via* NEXAFS. American Physical Society,APS March Meeting, March 15−19, 2010, abstract #B16.005.
42. Moon, J. S.; Takacs, C. J.; Cho, S.; Coffin, R. C.; Kim, H.; Bazan, G. C.; Heeger, A. J. Effect of Processing Additive on the Nanomorphology of a Bulk Heterojunction Material. *Nano Lett.* **2010**, *10*, 4006–4008.
43. Ratheesh, P. M. K.; Kartha, C. S.; Vijaykumar, K. P.; Singh, F.; Avasthi, D. K. Effect of Fluorine Doping on Structural, Electrical and Optical Properties of ZnO Thin Films. *Mater. Sci. Eng., B* **2005**, *117*, 307–312.